

PROPERTIES OF THE INTERGALACTIC MAGNETIC FIELD CONSTRAINED BY GAMMA-RAY OBSERVATIONS OF GAMMA-RAY BURSTS

P. VERES¹, C. D. DERMER², K. S. DHUGA

Department of Physics, George Washington University, Washington, D.C. 20052

¹Present address: Center for Space Plasma and Aeronomic Research, University of Alabama, Huntsville, AL 35899

²Also, School of Physics, Astronomy, and Computational Sciences, George Mason University, Fairfax, VA 22030

ABSTRACT

The magnetic field in intergalactic space gives important information about magnetogenesis in the early universe. The properties of this field can be probed by searching for radiation of secondary e^+e^- pairs created by TeV photons, that produce GeV range radiation by Compton-scattering cosmic microwave background (CMB) photons. The arrival times of the GeV “echo” photons depend strongly on the magnetic field strength and coherence length. A Monte Carlo code that accurately treats pair creation is developed to simulate the spectrum and time-dependence of the echo radiation. The extrapolation of the spectrum of powerful gamma-ray bursts (GRBs) like GRB 130427A to TeV energies is used to demonstrate how the IGMF can be constrained if it falls in the $10^{-21} - 10^{-17}$ G range for a 1 Mpc coherence length.

1. INTRODUCTION

Magnetic fields are ubiquitous in cosmic sources ranging from stellar mass objects to clusters of galaxies. Little information is known, however, about the intergalactic magnetic field (IGMF) on the largest scales of the voids. The properties of the IGMF, which are linked to cosmological structure formation (Neronov & Semikoz 2009), result from processes in the early universe or by expulsion of magnetic flux from structured regions. The characterization of the IGMF is crucial to assess magnetogenesis and effects of structure formation. Multiple spectral (Neronov & Vovk 2010), angular (e.g., Dolag et al. 2009; Ando & Kusenko 2010), and temporal (Plaga 1995) methods have been devised to constrain the magnitude of the average value of the IGMF, B_{IGMF} . Here we examine the temporal method involving delayed echo emission from GRBs.

Although we confine our study to GRBs, the method is in principle applicable to any flaring TeV source. The scenario considered here consists of TeV range source photons interacting with the extragalactic background light (EBL) photons, creating e^+e^- pairs. The pairs lose energy by Compton scattering CMB photons to the GeV range. Because of the magnetic deflection of the pairs, off-axis TeV photons generate GeV range γ -rays that travel to the observer on longer path lengths resulting in a “pair echo”, delayed compared to the prompt emission. The delay time method was first presented in Plaga (1995) and later developed in papers by Razzaque

et al. (2004), Murase et al. (2008), Ichiki et al. (2008), and Takahashi et al. (2011).

The coherence length R_{coh} characterizing the distance over which the IGMF changes direction by $\approx 90^\circ$, is a second important property of the IGMF. Because the coherence length in intergalactic space is so poorly known, the γ -ray techniques jointly constrain B_{IGMF} and R_{coh} , rather than each individually.

While there are no direct measurements of very high energy (VHE; $E \gtrsim 0.1$ TeV) radiation from GRBs, there are candidate events that under favorable observing conditions might have produced a detection. The spectrum of GRB 941017 (González et al. 2003) had a hard power law extending to $\gtrsim 100$ MeV with no turnover, in addition to the usual Band function describing the MeV emission. Similar hard power laws extending to multi-GeV energies have been discovered by Fermi in the case of GRB 090902B ($z = 1.822$) (Abdo 2009), GRB 090926A ($z = 2.106$) (Ackermann & the Fermi collaboration 2011), and GRB 130427A ($z = 0.34$) (Ackermann et al. 2014). The direction towards GRB 130427A was observed with VERITAS (Aliu et al. 2014), but the observing conditions were unfavorable and no VHE detection was made.

For the redshift range $z \gtrsim 0.3$, where most GRBs are detected, the pair formation optical depth of TeV photons with EBL photons is $\gg 1$, so VHE emission from high-redshift GRBs would be strongly attenuated. Indeed, the highest energy GRB photons yet measured, for example, the 95 GeV photon from GRB 130427A

arXiv:1705.08531v1 [astro-ph.HE] 23 May 2017

measured a few minutes after the burst trigger, are detected from relatively low redshift GRBs. GRBs are therefore reasonable candidates for TeV-range emission arising from either internal or external shocks, though we must assume that the hard GeV component continues uninterrupted up to photon energies $E \gtrsim 1$ TeV.

In this paper, we present Monte Carlo simulations of the above mentioned process for pair echo emission. The simulation assigns pair energies following their proper distribution so the pairs don't necessarily take half of the TeV photon's energy, a point often neglected in the literature. We give detection prospects for GRB echo radiation by the *Fermi* Large Area Telescope, by existing air and water Cherenkov telescopes, and by the future Cherenkov Telescope Array (CTA). We employ a threefold approach to constrain the value of the IGMF. We examine the echo radiation observables for the extremely bright GRB 130427A, and the detection prospects for Cherenkov telescopes at TeV energies for this same GRB. We also consider long exposure observations of GRBs with hard high-energy spectral components.

Our calculations are made for a flat Λ CDM cosmology with $\Omega_m = 0.27$, $\Omega_\Lambda = 0.73$, and $H = 72 \text{ km s}^{-1} \text{ Mpc}^{-1}$. For simplicity we use the terms pairs and electrons interchangeably. For quantity Q , we use the $Q_x = Q/10^x$ scaling notation. Physical constants have their usual notation. In Section 2 we review the analytic approach, and in Section 3 we describe our Monte Carlo simulation. Results are presented in Section 4, and we discuss and conclude in Section 5.

2. ANALYTIC CONSIDERATIONS

2.1. VHE photons

The source, in our case a GRB, emits TeV range ($0.1 \lesssim E = E_{\text{TeV}} \text{ TeV} \lesssim 100 \text{ TeV}$) photons which interact with EBL photons on the pair-production distance scale $\lambda_{\gamma\gamma}(E)$. This can be calculated for a specific EBL model that provides an optical depth $\tau(E, z)$ at photon energy E and redshift z , noting that $\lambda_{\gamma\gamma}(E) \cong D/\tau(E, z)$, where D is the distance to the source.

This interaction yields an electron-positron pair, each with Lorentz factor $\gamma_e = 10^6 \gamma_6$ and energy $E_e = m_e c^2 \gamma_e$, that are *on average* half of the energy of the TeV range photon, so that $\gamma_6 \approx E_{\text{TeV}}$. These pairs interact with the CMB photons and lose energy through inverse Compton (IC) scattering. The electron has a mean free path $\lambda_e = (n_{\text{CMB}} \sigma_T)^{-1} = 0.40 \text{ kpc} (1+z)^{-3}$ between scatterings, where $n_{\text{CMB}} \approx 409 (1+z)^3 \text{ cm}^{-3}$ is the CMB photon number density for temperature $T_{\text{CMB}} = 2.725 (1+z) \text{ K}$ (Fixsen 2009). The electrons lose their energy through repeated scatterings on a cool-

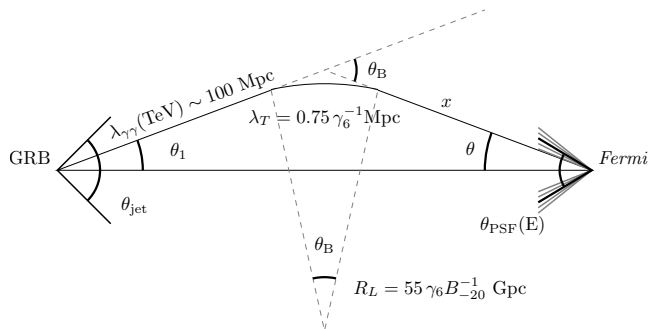


Figure 1. Schematic diagram of the scattering geometry. A photon from the GRB is emitted at angle θ_1 to the line of sight of an observer at distance D and pair produces by interacting with an EBL photon. The pairs with Larmor radius R_L in a uniform field of strength B cool on the length scale λ_T . Depending on the strength of the IGMF, the pairs may be deflected before cooling and so are able to emit GeV photons in the direction to the observer. The array of observing angles indicate the energy dependence of the point spread function (PSF) of Fermi/LAT.

ing length scale of

$$\lambda_T(\gamma_e) = \frac{m_e c^2}{\frac{4}{3} \sigma_T u_{\text{CMB}} \gamma_e} = 0.72 (1+z)^{-4} \gamma_6^{-1} \text{ Mpc}, \quad (1)$$

where $u_{\text{CMB}} \approx 4.2 \times 10^{-13} (1+z)^4 \text{ erg cm}^{-3}$ is the energy density of the CMB. Electrons with $\gamma_6 \approx 1$ scatter on the order of $\lambda_T/\lambda_e \sim 1000$ times before losing a substantial part of their energy. The upscattered photon's energy is $E_{\text{IC}} \approx 4/3 (2.7 k_B T_{\text{CMB}}) \gamma_e^2 \cong 0.8 \gamma_6^2 \text{ GeV}$. The scattering is in the Thomson regime provided $4\gamma_e(E/m_e c^2) \ll 1$, which implies that $\gamma_e \ll 2 \times 10^8$. Klein-Nishina effects therefore become important only for $\gtrsim 100 \text{ TeV}$ photons and, though we use the full Klein-Nishina kernel in our calculations, can be neglected in our study since the cut-off energy of the GRB emission is always assumed to be $\lesssim 30 \text{ TeV}$.

The process is sketched in Figure 1. The angle between the direction of the VHE photon, and the upscattered CMB photon is

$$\theta_B = \lambda_T/R_L = 1.3 \times 10^{-5} (1+z)^{-4} B_{-20} \gamma_6^{-2}, \quad (2)$$

where $R_L = \gamma m_e c^2 / q_e B = 55 \gamma_6 B_{-20}^{-1} \text{ Gpc}$ is the Larmor radius in a uniform field of strength $10^{-20} B_{-20} \text{ G}$. This equation is valid when the IGMF is coherent on scales larger than the IC cooling length λ_T , given by Equation 1. In the opposite case, the deflection angle is modified by a factor of $\sqrt{R_{\text{coh}}/\lambda_T}$, reflecting the random walk of the electron as it cools.

Following the notation of Dermer et al. (2011), the time delay of the echo photons arriving at the detector compared to the arrival time of photons that are emitted in the direction to the observer arrive can be calculated

from the differences in the path length, giving

$$c\Delta t = \lambda + x - D \approx \frac{1}{2}\lambda_{\gamma\gamma}\theta_B^2 \left(1 - \frac{\lambda_{\gamma\gamma}}{D}\right), \quad (3)$$

where $\lambda = \lambda_{\gamma\gamma} + \lambda_T \cong \lambda_{\gamma\gamma}$, and we have expressed x through the sine theorem: $x = D \sin \theta_1 / \sin \theta_B$ (see Figure 1).

Because the time delay can vary over many orders of magnitude depending on the values of B , R_{coh} , E , and z , it is instructive to give order-of-magnitude estimates for the time delay in specific cases. For $E = 0.5$ TeV and $z = 0.34$ (the redshift of GRB 130427A), we have $\lambda_{\gamma\gamma} \approx 700$ Mpc and $\Delta t \cong 0.3B_{20}^{-2}$ year. In the case of an $E = 10$ TeV photon, the mean free path for pair production with photons of the EBL is $\lambda_{\gamma\gamma} \approx 110$ Mpc and the time delay is $\Delta t \approx 9B_{-20}^2$ s.

3. MONTE CARLO SIMULATION

We have developed a code to calculate the echo flux from a source that emits VHE radiation with a known spectrum. The code follows the interaction of the photons with the EBL, the energy loss of the resulting pairs, and their deflection by the intergalactic magnetic field. Subsequently the pairs scatter CMB photons to produce emission in the energy range of the Fermi-LAT. We make the calculation by generating a population of pairs from the assumed GRB spectrum of TeV photons that interact with the EBL. We numerically integrate the IC contribution of pairs to obtain the desired observations. Instead of using the MC method for IC scattering, we numerically integrate the single electron IC emissivity to obtain the observed spectrum, because it is compu-

tationally more convenient.

As a geometrical problem (see Figure 1), the distance D to the source and the values of $\lambda_{\gamma\gamma}$ and θ_{diff} uniquely describe the configuration. Constraints such as requiring the photon emission angle to be within the opening angle the GRB jet ($\theta_1 < \theta_{jet}$), or requiring the arrival angle to be within the Fermi-LAT PSF ($\theta < \theta_{PSF}(E)$), are easy to apply. We assume that the jet axis is pointed towards us (see [Neronov et al. 2010](#), for a study of off-axis jets).

3.1. TeV range radiation

We generate a distribution of photons in the specified VHE energy range assumed to be described by a power-law distribution with high-energy cutoff. To mimic the EBL absorption and to select the population for pair creation we retain photons for which a randomly generated number (uniformly distributed between 0 and 1) exceeds $1 - e^{-\tau(E)}$. The distance at which each photon pair produces is drawn from a random exponential distribution with $\lambda_{\gamma\gamma}(E)$ as the average.

The TeV photons produce pairs by interacting with the EBL. For analytical calculations (e.g., [Dermer et al. 2011](#)) and some previous numerical treatments (e.g., [Takahashi et al. 2011](#); [Fitoussi et al. 2017](#)), it is customary to assume that the pairs equally share the energy of the parent TeV photon. Here we use the appropriate distribution function for the pairs from Equation (B1) in [Zdziarski \(1988\)](#). The distribution in energies of an electron with energy γ_e , given a VHE photon with energy $\epsilon m_e c^2$, is given by

$$P(\gamma_e, \epsilon) = \int_{\frac{\epsilon}{4\gamma_e\gamma'_e}}^{\infty} d\epsilon_{EBL} n(\epsilon_{EBL}) \frac{3\sigma_{TC}}{4\epsilon^2\gamma} \left(r - (2+r) \frac{\epsilon}{4\epsilon_{EBL}\gamma_e\gamma'_e} + 2 \left(\frac{\epsilon}{4\epsilon_{EBL}\gamma_e\gamma'_e} \right)^2 + \frac{\epsilon}{2\epsilon_{EBL}\gamma_e\gamma'_e} \ln \frac{4\epsilon_{EBL}\gamma_e\gamma'_e}{\epsilon} \right), \quad (4)$$

where $\gamma'_e = \epsilon - \gamma_e$, $r = (\gamma_e/\gamma'_e + \gamma'_e/\gamma_e)/2$, and ϵ_{EBL} and n_{EBL} are the EBL photon energy and number density, respectively, provided in [Finke et al. \(2010\)](#). For different VHE photon energies, the distribution is plotted in Figure 2. The average value is indeed at $\gamma_e = \epsilon/2$. At energies \gtrsim TeV, however, the distribution of secondary pairs starts to become increasingly unequal. For each VHE photon with energy $E_{TeV} = \epsilon m_e c^2$, we draw from this distribution and retain γ_e and γ'_e .

The pairs travel an average distance λ_T before losing their energy by scattering CMB photons. In our simulation, we again draw from an exponential distribution with $\lambda_T(\gamma_e)$ as the mean. Only one generation of secondaries is followed. The Compton-scattered radia-

tion may again be susceptible to pair attenuation by the CMB for the highest energy photons. For the 30 TeV maximum energy of GRB photons assumed in this study, the second generation emission in most of the cases can be neglected. The most energetic echo photons come from the more energetic original photons, which interact with the EBL, close to the source, namely at the same redshift. Where appropriate, we apply EBL absorption to the echo spectrum. We use the model described in ([Finke et al. 2010](#)) for the EBL, which is similar to currently favored models ([Biteau & Williams 2015](#); [Stecker et al. 2016](#)).

3.2. Flux

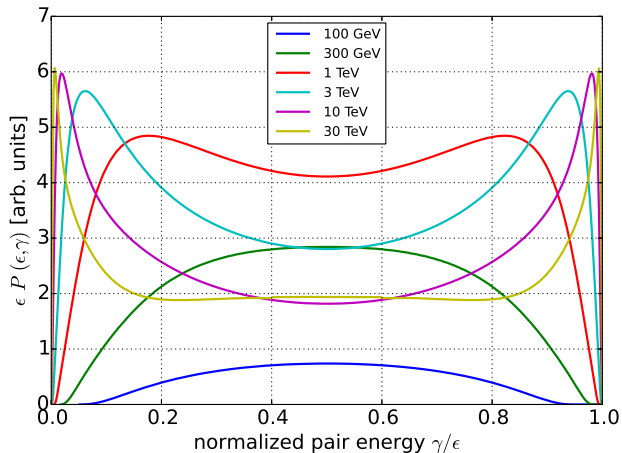


Figure 2. The normalized distribution of created pairs' energy from VHE photons with different energies interacting with the CMB.

The differential distribution of pairs created from the interaction of TeV photons with the EBL is denoted by $dN_0(\gamma_e)/d\gamma_e$. The echo radiation spectrum is calculated by integrating the electron IC power over the electron distribution using the expression

$$\frac{d^2 N_{\text{echo}}}{dE_{\text{IC}} dt} = \int d\gamma_e \frac{dN(\gamma_e)}{d\gamma_e} \frac{d^2 N_{E,\text{IC}}}{dE dt}. \quad (5)$$

The single electron power when scattering CMB photons is

$$\frac{d^2 N_{E,\text{IC}}}{dE dt} = \frac{3\sigma_{TC}}{4\gamma_e^2} \int \frac{dE_{\text{CMB}}}{E_{\text{CMB}}} n_{E,\text{CMB}} f(x), \quad (6)$$

where $f(x) = 2x \ln x + x + 1 - 2x^2$ and $x = \epsilon m_e c^2 / 4\gamma_e^2 E_{\text{CMB}}$ (Blumenthal & Gould 1970). The time integrated IC photon flux can be obtained by multiplying Eq. (6) with the local IC cooling time of the pairs:

$$\Delta t'_{\text{IC}}(\gamma_e) = \frac{m_e c^2}{\frac{4}{3}\gamma_e \sigma_{TC} u_{\text{CMB}}} = 7.3 \times 10^{13} \gamma_e^{-1} \text{ s} \quad (7)$$

(Fan et al. 2004).

In the analytic treatment of this problem, we need to link the distribution of the electrons ($dN_0/d\gamma_e$) to the pairs that contribute within the observing window ($dN/d\gamma_e$) (e.g. Dai & Lu 2002; Dai et al. 2002; Razzaque et al. 2004). To accomplish this, one has to consider the maximum timescale $\Delta t_{\text{obs}}(\gamma)$ of the angular, magnetic-deflection, IC-cooling, and GRB timescales as a function of γ_e (Razzaque et al. 2004), giving $dN/d\gamma_e = (\Delta t'_{\text{IC}}/\Delta t_{\text{obs}}(\gamma))dN_0/\gamma_e$ (Dai et al. 2002). In a numerical treatment of this process (Takahashi et al. 2011), the integration is performed between the locations of pair production and energy loss, provided that the deflection angle is sufficient for radiating emission into the observer's direction.

By contrast, in the MC approach used here we start from the distribution of pairs generated using Equation (4) and shown in Figure 2. We select those individual electrons whose associated delay time matches the observational criteria, and then calculate their contribution to the echo radiation.

We assume the source emits photons with a power law spectrum up to E_{cut} , which we typically choose to be 3 or 30 TeV in our examples. Photons from this spectrum are absorbed by the EBL. We calculate the isotropic equivalent energy absorbed from the difference between the unabsorbed and the absorbed fluxes (as shown in the numerical calculations below).

$$\mathcal{E}_{\text{abs}} = \int_{10 \text{ GeV}}^{E_{\text{cut}}} E \frac{dN(E)}{dE} (1 - e^{-\tau(E,z)}) dE. \quad (8)$$

The lower limit on the integration is set because the universe is transparent to 10 GeV photons at all redshifts since the epoch of galaxy formation ($z \sim 10$). The number of pairs involved in our simulations is $\mathcal{O}(10^5)$, but varies for different calculations. We use the total absorbed energy \mathcal{E}_{abs} to scale our simulation to the actual differential distribution of pairs. The simulated differential pair distribution is related to the real distribution through a scale factor C from the expression

$$C \int_1^{\infty} d\gamma_e (dN_{\gamma_e}/d\gamma_e)_{\text{sim}} \gamma_e m_e c^2 = C \sum_{i=1}^{N_{\text{pairs}}} \gamma_i m_e c^2 = \mathcal{E}_{\text{abs}}. \quad (9)$$

Next, we apply the observational criteria specifying start and stop times of observations. We choose the number of TeV photons, the cut energy E_{cut} , z , B_{IGMF} , and R_{coh} . We calculate $\lambda_{\gamma\gamma}$ and λ_T . Using these values, we determine θ_{diff} and the time delay Δt . We calculate the individual electrons' contribution to the spectrum and sum. Although we follow individual electrons, the resulting spectrum will be smooth, because we convolve the electron distribution with the Compton kernel.

3.3. Geometry

The observing angle θ of IC photons with energy E_{GeV} GeV that reach the observer can be calculated from the relation $\sin \theta = (\lambda_{\gamma\gamma}/D) \sin \theta_{\text{diff}}$. In order to be observed by Fermi, this angle has to be less than the energy dependent PSF of the LAT. For this, we use the expression $\theta_{\text{PSF}} \approx 1.68^\circ E_{\text{GeV}}^{-0.77} + 0.2^\circ e^{-10 E_{\text{GeV}}^{-1}}$, which is an analytical approximation for the 95 % containment PSF that is sufficiently accurate for our purposes (see Ackermann et al. 2013, for a detailed discussion of the Fermi PSF). This constraint is important for large IGMF values $\gtrsim 10^{-17}$ G. Neglecting this effect can introduce inaccuracies into the low-energy part of the echo radiation

spectrum.

4. COMPARISON WITH OBSERVATIONS

There is a variety of available data and possible future observing scenarios that can be useful in constraining the IGMF. Since we require VHE photons from a transient source, the best candidates are GRBs with hard power law spectral components in addition to the usual sub-MeV prompt spectrum.

Fermi LAT is an all-sky instrument (Atwood et al. 2009) sensitive in the 30 MeV – 300 GeV range. Currently VERITAS (Horan et al. 2005), HESS (Aharonian et al. 2004), and MAGIC (Aleksić et al. 2012) are the main air Cherenkov observatories with pointing capabilities. HAWC (Abeyssekara et al. 2013) is the largest operating water Cherenkov instrument that, though it does not allow pointing, has a large field of view and a nearly 100% duty cycle compared to the $\sim 10\%$ duty cycle of current imaging air Cherenkov telescopes. The Cherenkov Telescope Array, (CTA Actis et al. 2011), will usher in a new era in VHE astrophysics by having a sensitivity approximately an order of magnitude greater than current air Cherenkov telescopes.

4.1. Spectral and temporal evolution

To assess if our code behaves correctly, we calculate the time evolution of the echo flux for a cutoff of 3 TeV. Fig. 3 shows results of our calculations for $B = 10^{-20}$ G. Here and throughout we fix the coherence length of the magnetic field to $R_{\text{coh}} = 1$ Mpc, while recognizing that this is poorly known quantity. Derivations with different R_{coh} can be calculated, however, since our data consists of upper limits, we focus this study on the IGMF for an assumed value of R_{coh} to demonstrate the method.

The spectra at different times have a low-energy power-law segment followed by a break and a rapidly dropping flux (Fig. 3, top). The echo spectrum at low energies behaves roughly as $\nu F_\nu \propto E^{1.5}$, corresponding to a cooling spectrum of a narrow electron distribution injected at high energies. The evolution of the break with time is a consequence of the more rapid re-processing of higher energy photons, which make higher energy pairs that are less deflected by the IGMF, so that the higher-energy Compton-scattered photons have a shorter path length to the observer.

Fig. 3 (bottom) shows the passing of the spectral peak in different energy bands. At lower energies the power law slope is shallower and the break occurs later. The peak of the νF_ν spectrum decreases $\propto t^{-1}$. This behavior broadly follows from the fact that the total echo fluence ($F \times t$) is determined by the amount of VHE flux absorbed by the EBL and is constant.

4.2. GRB 130427A and VERITAS constraints

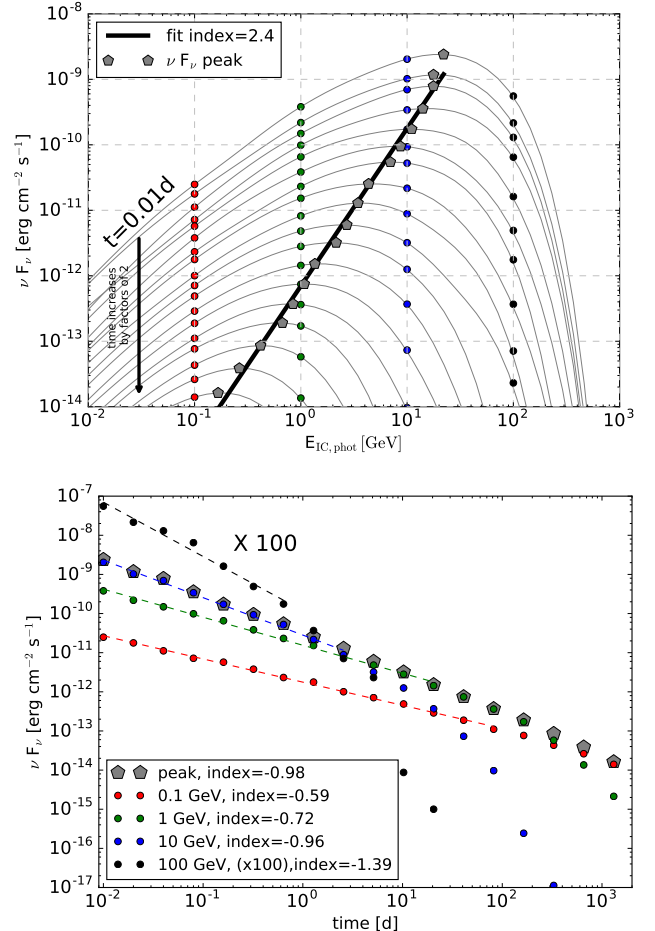


Figure 3. Time evolution of the echo radiation for $B = 10^{-20}$ G and $R_{\text{coh}} = 1$ Mpc. The source of VHE photons (the “C” interval of GRB 130427A, see Figure 4) is omitted for clarity. The top figure shows echo spectra recorded at 0.01, 0.02, 0.04 ... days after the trigger, with the lowest curve at 1310 days. Gray pentagons mark the maximum of the spectra, $(\nu F_\nu)_{\text{peak}} \propto E_{\text{IC,peak}}^{2.4}$. The bottom figure shows the lightcurve at different energies and at the peak, where we have $(\nu F_\nu)_{\text{peak}} \propto t^{-0.98}$.

GRB 130427A had the largest γ -ray fluence of any GRB yet observed, with high-energy emission detectable up to ~ 1 day after the burst trigger with Fermi LAT. VERITAS followed up and derived an upper limit for the flux at 100 GeV at 0.82 days after the trigger (Aliu et al. 2014). Here, we use the VERITAS upper limit to place constraints on the IGMF. We use the emission episode from 11.5 – 33 s after the burst trigger, where the spectrum can be described as a power law with photon index $\Gamma = -1.66 \pm 0.13$, to define the γ -ray spectrum from this GRB. Since there was no sign of a spectral cutoff, we assume the spectrum extended up to 3 and 30 TeV to give estimates for the echo radiation flux.

In Figure 4 we calculate the echo radiation using our simulation and compare it with the VERITAS measure-

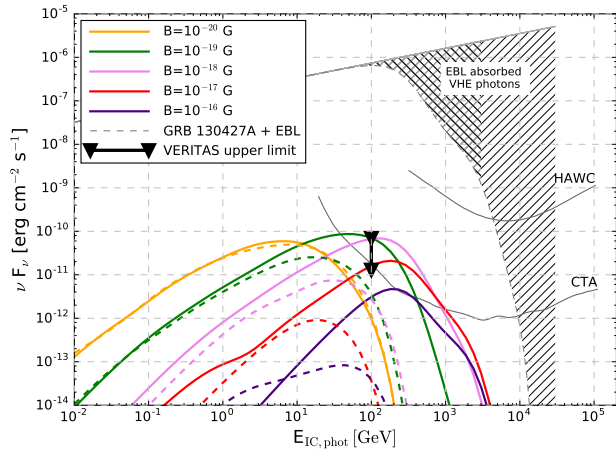


Figure 4. Simulated echo spectra assuming that the echo radiation is seeded by an extrapolation of the GRB emission spectrum measured in interval “C” ($\Delta t = 21.5$ s) of the lightcurve of GRB 130427A (Ackermann et al. 2014) to TeV energies. Numerical results with assumed cutoff energies of 3 and 30 TeV are shown by the heavy dashed and solid curves, respectively, are compared with VERITAS upper limit for GRB 130427A. The range of upper limits indicates different assumed spectral index. The coherence length of the IGMF is assumed to be $R_{\text{coh}} = 1$ Mpc.

ments. VERITAS provides a range of upper limits based on the assumed spectral shape. By comparing the VERITAS limits with the simulated spectra, we find that either $B_{\text{IGMF}} \gtrsim 10^{-17}$ G or $B_{\text{IGMF}} \lesssim 3 \times 10^{-19}$ G for the $E_{\text{cut}} = 30$ TeV case (otherwise the calculated echo flux would violate the VERITAS upper limits). The $E_{\text{cut}} = 3$ TeV case does not give any constraints. Based on current estimates for CTA sensitivity, more stringent constraints are expected for observations similar to that of VERITAS (see Figure 4). HAWC is more likely to observe the direct prompt radiation than the echo flux.

4.3. GRB 130427A and Fermi-LAT constraints

Another intriguing method to constrain the IGMF is provided by Fermi-LAT observations of GRB 130427A. The $E = 32$ GeV photon observed at $\Delta t = 34.4$ ks after the GRB trigger is difficult to interpret in the framework of synchrotron radiation from the forward shock (Ackermann et al. 2014). Nonetheless it might be associated with an IC component, even though there is no evidence for the spectral and temporal break expected for a transition from synchrotron to Compton emission.

If we assume this photon originates from the echo radiation, there is a straightforward way to estimate the IGMF using Equation (3). A simple calculation yields $B_{\text{IGMF}} = 2.2 \times 10^{-19} (\Delta t / 34.4 \text{ ks})^{1/2} (\lambda_{\gamma\gamma} / 146 \text{ Mpc})^{-1/2} ((1+z)/1.34)^4 (E/32 \text{ GeV}) \text{ G}$ with $\lambda_{\gamma\gamma} \approx 150$ Mpc and $E \sim 6.3$ TeV as the energy of the primary photon.

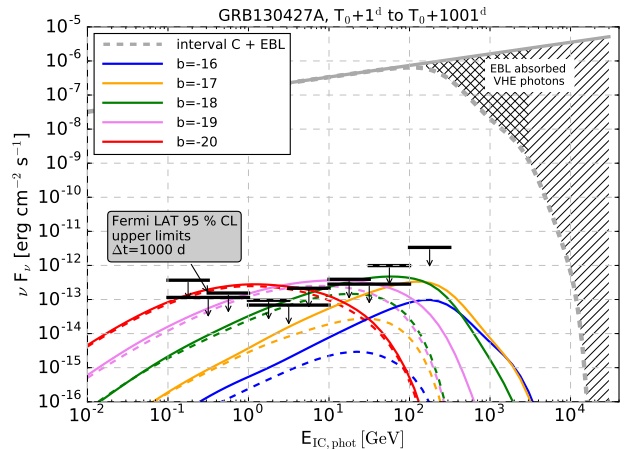


Figure 5. Long exposure observations with Fermi-LAT in the direction of GRB 130427A give the upper limits shown for detection between 1 and 1001 days after the GRB as a function of photon energy for different values of b , where the IGMF $B = 10^b$ G. Calculations show echo spectrum for cutoff energies of 3 and 30 TeV vs. photon energy, represented by dashed and continuous lines, respectively.

Equation (3) can be solved by Monte Carlo methods to gauge the error on this IGMF value, and we get $\log_{10} B_{\text{IGMF}} = -18.8 \pm 0.3$. This represents the average of the simulated values and it differs somewhat from the estimated value, partly due to the asymmetry of the distribution of simulated values.

4.4. Long temporal baseline observations

The delayed echo radiation potentially lasts for a long time compared to the time during which high-energy GRB afterglow radiation is expected. Since Fermi-LAT is an all sky monitor, we explore the possibility that the echo radiation can be detected with long exposure observations starting from one day after the GRB to several years, on the order of the lifetime of Fermi/LAT. We therefore calculated the flux of the echo radiation from GRB 130427A for observations starting one day after the GRB, where the direct GeV range afterglow radiation already went undetected. This observation spans 1000 days (see Figure 5).

To compare the simulated echo spectrum with observations, we use Fermi-LAT data, specifically PASS 8 photons with P8R2_SOURCE_V6 filters. The diffuse galactic foreground was accounted for using `gll_iem_v6`, and the isotropic diffuse radiation by `iso_P8R2_SOURCE_V6`. We used the `fermipy`¹ package and its routines to derive Fermi-LAT upper limits.

Fermi LAT upper limits for the long term (1000 d) observations in the direction of GRB 130427A are on

¹ <http://fermipy.github.io> (version 0.13.2)

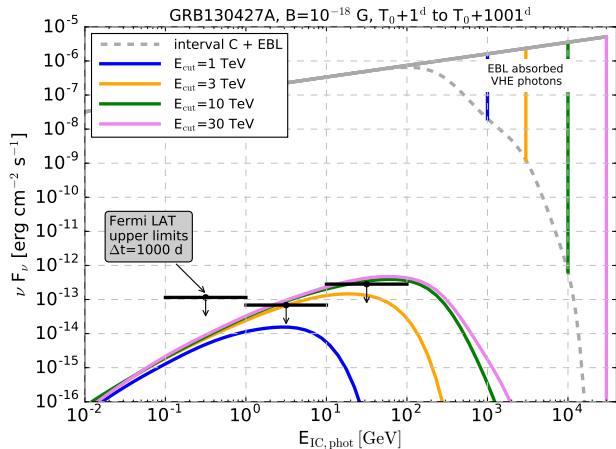


Figure 6. Calculation to determine the cutoff energy E_{cut} for a GRB similar to GRB 130427A, assuming $B = 10^{-18}$ G and $R_{\text{coh}} = 1$ Mpc. Different values of E_{cut} are shown in the legend and the corresponding echo spectrum is drawn with the same color.

the order of 10^{-13} erg cm $^{-2}$ s $^{-1}$ (see Figure 5 for the exact values). By comparing the upper limits to the MC simulations, we can rule out the cases where $10^{-18} \gtrsim B_{\text{IGMF}}(\text{G}) \lesssim 10^{-20}$. Stronger magnetic fields ($B_{\text{IGMF}} \gtrsim 10^{-17}$ G) do not violate the upper limits.

4.5. Cutoff energy

The power-law spectral components with photon index harder than -2 will have a cutoff energy. This cutoff energy of the delayed hard component is generally outside of the Fermi LAT range. To gauge the effects of different cutoff energies, here we use Fermi LAT observations starting from one day after the GRB trigger, where the afterglow has faded, ending at 1001 days after (similarly to the previous subsection). In Figure 6 we make a calculation of the echo radiation using the parameters of GRB 130427A, with varying cutoff energies, assuming a magnetic field strength of 10^{-18} G. This is near the lower limit of the IGMF inferred from observations of blazars (Dermer et al. 2011). We overplot the expected echo radiation with different cutoff energies and show that long-term LAT observations provide meaningful constraints assuming this value of B . In particular for $B = 10^{-18}$ G, $E_{\text{cut}} \gtrsim 3$ TeV the predicted echo flux violates the LAT upper limits.

5. DISCUSSION AND CONCLUSION

We have investigated the use of GRBs for constraining the IGMF using the Fermi-LAT and existing and future Cherenkov telescopes. We assume GRBs emit radiation in the TeV range, with pairs produced through $\gamma\gamma$ pair creation of the VHE γ rays interacting with EBL photons. These pairs Compton-scatter EBL photons (here,

we use the model of Finke et al. (2010)) to GeV energies to make a delayed echo radiation. We find Fermi LAT can constrain the radiation from powerful GRBs like GRB 130427A if the IGMF is in the $10^{-21} - 10^{-17}$ G range, assuming a 1 Mpc coherence length. Depending on the assumed spectrum and cutoff energy of the TeV spectral component, this range could be broader. We have also shown how the VERITAS non-detection of this GRB can constrain B and the cutoff energy of the TeV spectrum.

Spectral methods to constrain the IGMF have been successfully applied in studies of blazars (D’Avezac et al. 2007; Neronov & Semikoz 2009; Dolag et al. 2011; Dermer et al. 2011; Finke et al. 2015) for which the VHE spectrum can be directly measured. Making the most conservative assumption that the blazar is operating for no longer than the time over which high-energy γ -ray emission has been observed, values of $B \gtrsim 10^{-19} - 10^{-18}$ G are inferred for a 1 Mpc coherence length of the IGMF. This lower limit of the IGMF is in the regime where pair echo radiation from GRBs can be detected, and we have shown that echo radiation should be detected if the cutoff energy is $\gg 1$ TeV for a GRB 130427A-type GRB.

The inferences of the values of the IGMF from blazar studies is, like the GRB case, very sensitive to the spectrum at the highest energies which cannot be detected either due to sensitivity limitations or attenuation by the EBL. Thus Arlen et al. (2014) conclude that the blazar data is compatible with an arbitrarily weak IGMF.

The main advantage of GRBs for the temporal method of inferring the IGMF lies in the transient nature of the direct emission. In the case of blazars, the echo radiation is superposed on the direct emission, whereas for GRBs the prompt emission fades away. The fading afterglow in the GeV range may still, however, be confused with the echo radiation. Murase et al. (2009) discusses the possible confusion between the echo and direct emission. A further pertinent issue for the inference of the IGMF from blazar studies is whether collective effects from the beamed pairs extract the energy of the e^+ and e^- more quickly than IC processes (e.g., Broderick et al. 2012; Chang et al. 2012; Schlickeiser et al. 2012; Menzler & Schlickeiser 2015). Depending on the relative densities of the beam and background plasma, the duration of the source, and pair spectrum, this energy can be extracted due to linear two-stream instabilities. This issue, which is important for persistent sources like blazars, is not so severe for a transient GRB source.

Fermi-LAT is the best suited instrument to probe the GeV range data produced by the pair echo. For a wide range of parameters likely to apply to this problem (e.g. the value of B , the TeV-range spectrum of the GRB emission, and the coherence length), the peak of the echo spectrum falls in the Fermi-LAT range. With the

advent of HAWC and the upcoming CTA, searches for echo emission from GRBs will provide more stringent constraints on the IGMF.

Acknowledgments: We thank Matthew Wood for prompt help using *fermipy*. PV acknowledges support from Fermi grant NNM11AA01A and thanks OTKA NN 111016 grant for partial support.

REFERENCES

- Abdo, A. A. e. a. 2009, *ApJ*, 706, L138
- Abeysekara, A. U., Alfaro, R., Alvarez, C., et al. 2013, *ArXiv e-prints*, arXiv:1306.5800
- Ackermann, M., & the Fermi collaboration. 2011, *ApJ*, 729, 114
- Ackermann, M., Ajello, M., Allafort, A., et al. 2013, *ApJ*, 765, 54
- Ackermann, M., Ajello, M., Asano, K., et al. 2014, *Science*, 343, 42
- Actis, M., Agnetta, G., Aharonian, F., et al. 2011, *Experimental Astronomy*, 32, 193
- Aharonian, F., Akhperjanian, A., Beilicke, M., et al. 2004, *ApJ*, 614, 897
- Aleksić, J., Alvarez, E. A., Antonelli, L. A., et al. 2012, *Astroparticle Physics*, 35, 435
- Aliu, E., Aune, T., Barnacka, A., et al. 2014, *ApJ*, 795, L3
- Ando, S., & Kusenko, A. 2010, *ApJ*, 722, L39
- Arlen, T. C., Vassilev, V. V., Weisgarber, T., Wakely, S. P., & Yusef Shafi, S. 2014, *ApJ*, 796, 18
- Atwood, W. B., Abdo, A. A., Ackermann, M., et al. 2009, *ApJ*, 697, 1071
- Biteau, J., & Williams, D. A. 2015, *ApJ*, 812, 60
- Blumenthal, G. R., & Gould, R. J. 1970, *Reviews of Modern Physics*, 42, 237
- Broderick, A. E., Chang, P., & Pfrommer, C. 2012, *ApJ*, 752, 22
- Chang, P., Broderick, A. E., & Pfrommer, C. 2012, *ApJ*, 752, 23
- Dai, Z. G., & Lu, T. 2002, *ApJ*, 580, 1013
- Dai, Z. G., Zhang, B., Gou, L. J., Mészáros, P., & Waxman, E. 2002, *ApJ*, 580, L7
- D’Avezac, P., Dubus, G., & Giebels, B. 2007, *A&A*, 469, 857
- Dermer, C. D., Cavadini, M., Razzaque, S., et al. 2011, *ApJ*, 733, L21
- Dolag, K., Kachelrieß, M., Ostapchenko, S., & Tomàs, R. 2009, *ApJ*, 703, 1078
- Dolag, K., Kachelriess, M., Ostapchenko, S., & Tomàs, R. 2011, *ApJ*, 727, L4
- Fan, Y. Z., Dai, Z. G., & Wei, D. M. 2004, *A&A*, 415, 483
- Finke, J. D., Razzaque, S., & Dermer, C. D. 2010, *ApJ*, 712, 238
- Finke, J. D., Reyes, L. C., Georganopoulos, M., et al. 2015, *ApJ*, 814, 20
- Fitoussi, T., Belmont, R., Malzac, J., et al. 2017, *MNRAS*, 466, 3472
- Fixsen, D. J. 2009, *ApJ*, 707, 916
- González, M. M., Dingus, B. L., Kaneko, Y., et al. 2003, *Nature*, 424, 749
- Horan, D., Badran, H. M., Blaylock, G., et al. 2005, in *American Institute of Physics Conference Series*, Vol. 745, *High Energy Gamma-Ray Astronomy*, ed. F. A. Aharonian, H. J. Völk, & D. Horns, 591–596
- Ichiki, K., Inoue, S., & Takahashi, K. 2008, *ApJ*, 682, 127
- Menzler, U., & Schlickeiser, R. 2015, *MNRAS*, 448, 3405
- Murase, K., Takahashi, K., Inoue, S., Ichiki, K., & Nagataki, S. 2008, *ApJ*, 686, L67
- Murase, K., Zhang, B., Takahashi, K., & Nagataki, S. 2009, *MNRAS*, 396, 1825
- Neronov, A., Semikoz, D., Kachelriess, M., Ostapchenko, S., & Elyiv, A. 2010, *ApJ*, 719, L130
- Neronov, A., & Semikoz, D. V. 2009, *Phys. Rev. D*, 80, 123012
- Neronov, A., & Vovk, I. 2010, *Science*, 328, 73
- Plaga, R. 1995, *Nature*, 374, 430
- Razzaque, S., Mészáros, P., & Zhang, B. 2004, *ApJ*, 613, 1072
- Schlickeiser, R., Ibscher, D., & Supsar, M. 2012, *ApJ*, 758, 102
- Stecker, F. W., Scully, S. T., & Malkan, M. A. 2016, *ApJ*, 827, 6
- Takahashi, K., Inoue, S., Ichiki, K., & Nakamura, T. 2011, *MNRAS*, 410, 2741
- Zdziarski, A. A. 1988, *ApJ*, 335, 786